

Article

Enhanced Optically–Excited THz Wave Emission by GaAs Coated with a Rough ITO Thin Film

Anup Kumar Sahoo ¹, Shi-Ying Kang ¹, Peichen Yu ² and Ci-Ling Pan ^{1,*}¹ Department of Physics, National Tsing Hua University, Hsinchu 30013, Taiwan² Department of Photonics, National Yang Ming Chiao Tung University, Hsinchu 30010, Taiwan

* Correspondence: clpan@phys.nthu.edu.tw

Abstract: In this study, we report enhancement of terahertz (THz) radiation with indium-tin-oxide (ITO) thin-film deposited on semi-insulating gallium arsenide substrate (SI-GaAs). The amplitude of THz emission from both ITO/SI-GaAs and bare SI-GaAs substrate as a function of optical pump (i) incident angle, (ii) polarization angle, and (iii) power were investigated. The enhancement of peak amplitude of a THz pulse transmitted through the ITO/SI-GaAs sample in comparison to bare SI-GaAs substrate varied from 100% to 0% when the pump incidence angle changed from 0° to 50°. The maximum enhancement ratio of peak amplitude for a coated sample relative to the bare substrate is approximately up to 2.5 times at the minimum pump intensity of 3.6 TW/m² and gradually decreased to one at the maximum pump intensity of 20 TW/m². From outcomes of these studies, together with data on surface and material characterization of the samples, we show that THz emission originates from the ITO/GaAs interfaces. Further, both interface-field-induced transient current and field-induced optical rectification contribute to the observed THz signal. Observed enhancement was tentatively attributed to surface-plasmon-induced local field enhancement, coupled with constructive interference of forward and retro-reflected backward THz emission from the ITO/GaAs interfaces. The polarity-flip reported previously for very thin Au-coated GaAs was not observed. This was explained by the wide-bandgap, transparency and lower free carriers of ITO. For best results, the incident angle should be in the range of 0 to 30° and the incident polarization should be 0 to 45°. We further predict that the ITO thin film of suitable thickness or with engineered nanostructures, post-annealed under optimum conditions may lead to further enhancement of THz radiation from ITO-coated semiconductor surfaces.

Keywords: terahertz (THz); indium-tin-oxide (ITO); semi-insulating gallium arsenide (SI-GaAs); THz emission; surface and interface



Citation: Sahoo, A.K.; Kang, S.-Y.; Yu, P.; Pan, C.-L. Enhanced Optically–Excited THz Wave Emission by GaAs Coated with a Rough ITO Thin Film. *Coatings* **2023**, *13*, 461. <https://doi.org/10.3390/coatings13020461>

Academic Editor: Alexandre Botas

Received: 30 December 2022

Revised: 7 February 2023

Accepted: 10 February 2023

Published: 17 February 2023



Copyright: © 2023 by the authors. Licensee MDPI, Basel, Switzerland. This article is an open access article distributed under the terms and conditions of the Creative Commons Attribution (CC BY) license (<https://creativecommons.org/licenses/by/4.0/>).

1. Introduction

Currently, the terahertz (THz) band of the electromagnetic (EM) spectrum (0.1 to 10 THz, the so-called T-ray), also known as sub-millimeter wave or far-infrared (FIR) radiation, has drawn much attention due its fundamental importance and potential applications in a variety of fields [1–3]. The device technology associated with these studies has enabled an array of applications ranging from fundamental research to technology innovation and commercialization [4,5]. In particular, the THz frequency band has shown a tremendous advantage over the microwave and millimeter wave (MMW) band owing to its inherent higher data rates for the future wireless communication technology [6,7]. A highly efficient and complementary metal-oxide-semiconductor (CMOS)-based THz device has also been demonstrated for imaging [8].

Despite the tremendous importance and progress of THz Science and Technology (THz S&T), several issues are currently restricting its diverse application in scenarios including sixth-generation (6G) or beyond fifth-generation (5G) communication systems [9]. One of the primary concerns is related to THz emitters that currently are not offering all the needed

properties like high radiation power, broad spectral bandwidth, and gapless spectrum for practical applications [10]. State-of-art THz transmitters have been demonstrated with both bulk semiconductors and plasma oscillation thereof, quantum cascade lasers, optically pumped semiconductor, solid state devices, etc. [11–13].

Of these, ultrafast electromagnetic (EM) wave emission in the THz frequency band from an unbiased semiconductor surface or metal/semiconductor Schottky interfaces [14–17] is attractive, partly because the relevant physical mechanisms are universal and the generated THz beam is broad and easily collimated, suitable for imaging applications. THz emission from semiconductor surfaces excited by ultrafast laser pulses were reviewed by, e.g., Krotkus et al. [18] and Gu and Tani [19], while that from (nanostructured) metal surfaces were surveyed by Ramanandan et al. [20]. Briefly, generated THz can be written as, $E_{\text{THz}} \propto \partial^2 P / \partial t^2 + \partial J / \partial t$, where P is the instantaneous nonlinear polarization and J is the photoinduced transient current (Appendix A.9). The nonlinear polarization is a difference frequency generation process, often referred as optical rectification (Appendix A.5) as frequency mixing of the modes in ultrafast optical pulses with a spectrum spanning tens of THz leads to frequency mixing terms in the “dc” range, contributing to the formation of ultrafast electromagnetic transients which spectrum lie in the THz frequency band. The nonlinear optical response could be caused by second-order susceptibility in non-centrosymmetric crystals and/or third-order induced by an effective second-order susceptibility that is assisted by the built-in field (Appendix A.1) present at semiconductor surfaces or semiconductor/metal interfaces. The presence of the surface field, e.g., due to band bending that leads to the formation of a depletion region, can also drive the photo generated carriers and results in a transient surge current (Appendix A.7) as the source term for THz radiation. With a small surface-depletion field, narrow-bandgap semiconductors such as indium arsenide (InAs) and indium antimonide (InSb) can be effective THz emitters by taking advantage of the effective photo voltage developed by the much faster diffusion of electrons than holes, the so-called photo-Dember effect (Appendix A.3). It is possible to enhance the efficiency of semiconductor THz emitters through appropriate coating of their surfaces and taking advantage of the local field by the surface plasmonic effect (Appendix A.8). For instance, Ramakrishnan et al. [14], reported a THz field enhancement of more than an order of magnitude for a $\text{Cu}_2\text{O}/\text{Au}$ structure. Recently, with the development of advanced materials including graphene and related two dimensional (2D) materials, new opportunity for the realization of compact THz emitters has emerged. As of now, graphite, single-layer, and/or multilayer graphene and other layered transition-metal dichalcogenides such as Molybdenum disulfide (MoS_2), molybdenum diselenide (MoSe_2), and Tungsten diselenide (WSe_2) for coherent THz pulse radiation have been reported [15,21–23]. Surface THz radiation from these layered materials irradiated by femtosecond pulses were explained by the optical rectification and/or photocurrent induced by the surface depletion field and built-in field enhancement with the localized surface plasmons. However, there are great challenges to improve growth techniques and repeatability of those materials. Instability of the surface due to chemical degradation of the above novel coatings in ambient conditions and large-scale fabrication issues remain as fundamental barriers to their future prospects as effective THz emitters.

It is interesting to consider indium-tin-oxide (ITO) as an alternative to metals in metal/semiconductor THz emitters. ITO belongs to the family of transparent conducting oxides or TCO [24,25], an important coating material now widely used in consumer electronics, displays, smart windows, and solar cells. The dielectric and electrical properties of sputtered ITO films have been characterized from the visible to THz frequency range [26–28]. ITO is essentially transparent (~85%) at the wavelength of the widely available and reliable ultrafast Ti:sapphire laser (e.g., 800 nm), highly conductive for easy biasing. Its electrical and optical properties can be tuned by varying the percentage of Sn and the doping level [29], making it a promising alternative for plasmonic material [30]. Recently, several novel applications of ITO have emerged. Aithal et al. [31] observed maintenance of cell phenotype and long-term functionality of human dermal fibroblast (HDF) cells on

ITO modified by self-assembled monolayers (SAMs). This important advance is significant for the future development of bioengineered skins. Subacius et al. [32] studied the structural, optical, and electrical properties of super-thick (of the order of microns) ITO films. Such thick films are potentially useful as protective coatings for energy-collecting mirror-concentration systems in open atmosphere. Micron-scale ITO coatings have also been used as a medium for unconventional tailoring and manipulation of light-matter interaction, e.g., materials with zero permittivity (epsilon-near-zero) or metamaterials [33] for applications in optical communications, RF-photonics, and integrated silicon photonics. Similar materials like graphene oxides were recently demonstrated for plasmon-coupled soliton emission and engineered for biosensing applications [34].

In the 1990s, Jin et al. [35] and Li et al. [36] first studied metal/semiconductor surface THz emitters. They reported phenomena such as polarity reversal and an enhancement of emitted THz signals. A number of metals, including sputtered ITO thin film, on SI-GaAs substrate were investigated, although the physical properties and deposition methods of ITO films studied were not revealed in these earlier works. A qualitative picture based on the dipole radiation (Appendix A.2) in the depletion zone of the semiconductor and generalized Snell's law was used to explain the physical mechanism of the anomalous THz emission from unbiased ITO/SI-GaAs interfaces [36]. In a follow-up study, Shi et al. [37] showed that the polarity-flip only occurred for Au/GaAs when the pump intensity was sufficiently high, arising from the interplay surface fields in GaAs and Au during irradiation of ultrafast laser pulses. Later, X. Wu [38] explained the enhancement by the lateral Dember current [39] due to the inhomogeneity of cracks or percolation patterns in thin (~ 8 nm) Au films deposited on the GaAs substrate. The preliminary outcome on enhanced THz emission with thicker (~0.5 μm) ITO film deposited on GaAs has also been reported by us in a conference paper [40].

In this work, we have investigated THz emission from an unbiased SI-GaAs and ITO/SI-GaAs excited by femtosecond laser pulses using a transmission type experimental setup. To facilitate the physical understanding, the dielectric properties of ITO thin film and SI-GaAs in the frequency range of 0.2 to 1.2 THz have also been investigated using THz time domain spectroscopy (THz-TDS) data. In addition, enhancement of THz emission due to the ITO thin film as a function of optical pump incident angle, polarization, and power has been studied. New phenomena were observed. In particular, we have not observed the polarity flip. Besides the surge current by the interface (surface) field, we identify a nonlinear optical contribution to the emitted THz power. The saturation of THz emission at high pump intensity was observed and satisfactorily explained. We believe this study could have significant impacts on the development of next-generation THz emitters for various applications in science and technology.

This paper is organized as follows. First, Section 2, the materials and methods used are discussed. Next, we present in Section 3 results and discuss their significance in lengths. In Section 4 conclusions of the paper are then summarized. Finally, we briefly describe the terminologies used to aid interdisciplinary readers in the Appendix A.

2. Materials and Methods

2.1. Sample Preparation

We choose a two-side polished un-doped semi-insulating (SI)-GaAs substrate with resistivity of $1 \times 10^7 \Omega\text{-cm}$ and thickness of 350 μm for this study. Half of the substrate was covered with hard mask to deposit the ITO thin film on the other half of the substrate. The substrate was then attached to the holder in an electron gun (e-gun, FU-12PEB, F.S.E. Corp., New Taipei City, Taiwan) evaporation system. The target of the ITO source is composed of 5% tin oxide (SnO_2) and 95% of indium oxide (In_2O_3). Then, a ~243 nm thick ITO thin film was grown on half of the substrate at a deposition rate of 5–10 $\text{\AA}/\text{s}$ while the chamber maintained a base pressure down to 5×10^{-6} torr. No pre- or post-annealing was applied. Afterwards, a high-resolution scanning electron microscope (SEM, JSM-7000F, Japan Electron Optics Laboratory Co., Ltd., Mitaka, Tokyo) was used to investigate

surface morphology and thickness of ITO thin film. Energy-dispersive spectroscopy (EDS, FEI Helios Nanolab 600i System) and atomic force microscopy (AFM, SPA-300HV, Seiko) measurements were also conducted.

2.2. Transmission Type Experimental Setup for THz Emission

Figure 1 shows a home-made transmission type experimental setup employed for generation and detection of THz radiation from the samples under study. The excitation source is a Ti:sapphire regenerative Amplifier (RGA; Spectra Physics, Spitfire), which typically generated 60 fs duration pulses at a repetition frequency of 1 kHz and central wavelength of 810 nm. The pump beam was S-polarized and the samples were irradiated at a pulse energy up to 262 μJ . The probe beam and pump (exciting) beams were separated using a beam splitter (BS). Then, the pump beam was directed to the sample through a half wave plate (HWP), polarizing beam splitter (PBS), and a reflective mirror (RM). The pump beam power and incident angle were tuned using a HWP and a Brewster-angle polarizer, respectively. Additionally, another HWP allowed variation of the polarization angle of the pump beam. The emitted THz wave from the substrate and the sample were collected, collimated, and then focused onto the free-space electro-optic sampling (EOS) system [41] using a pair of off-axis mirrors (OAMs). The probe beam was aligned so that it co-propagated in the electro-optical (EO) crystal (500 μm -thick ZnTe), after being properly attenuated with a neutral density (ND) filter. The sample to be tested was placed on a rotation stage to allow investigation of the angle dependence of THz emission. The diameter of the exciting beam was measured to be approximately 3.5 mm. Experiments were carried out in a stable nitrogen environment to reduce the effect of water vapor absorption.

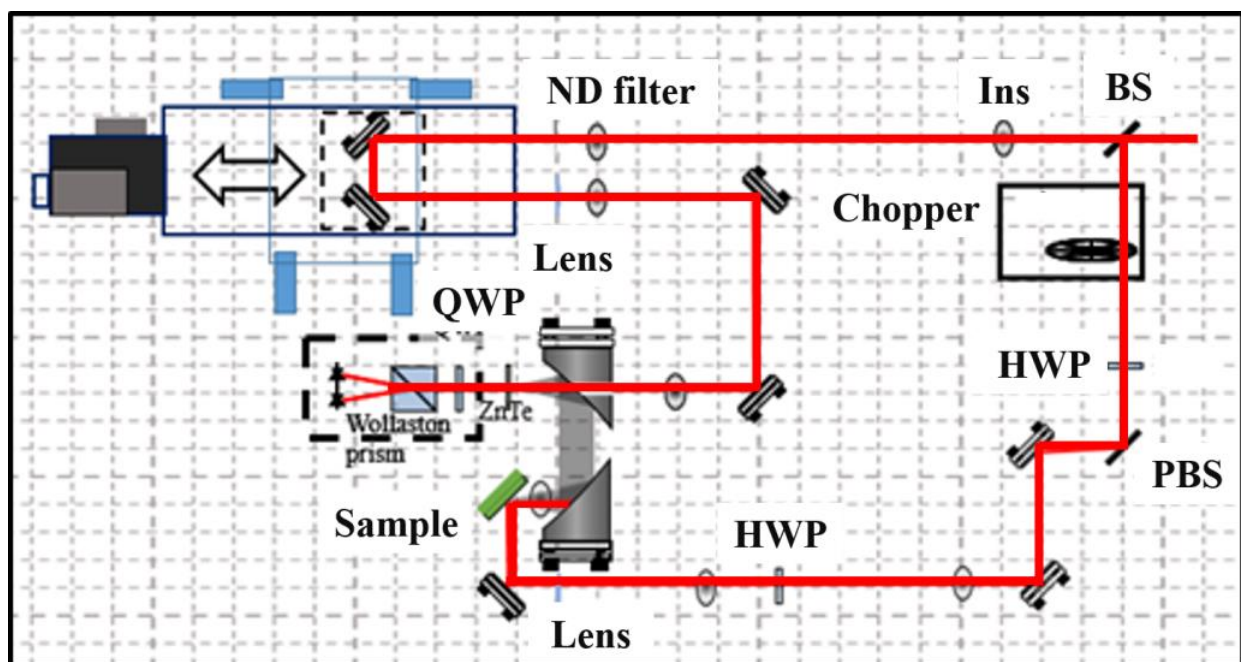


Figure 1. A transmission type THz emission setup (all abbreviations are explained in the text).

For the determination of THz optical constants of ITO thin film and bare Si-GaAs substrate, a typical photoconductive antenna-based transmission type THz time-domain spectrometer (THz-TDS) was employed which has been described in detail elsewhere [42]. A mode-locked Ti:sapphire laser (Spectra Physics, Tsumai) having an average power of ~ 0.4 W at a repetition rate of 82 MHz producing ~ 35 fs was used as the light source for such diagnostic. Its central wavelength and bandwidth were 800 nm and 43 nm, respectively.

3. Results and Discussion

In Figure 2a, we show a typical high-resolution SEM image of the top view of coated ITO film. The image revealed a moist and polycrystalline ITO thin film that was deposited on the SI-GaAs substrate. The image looks like an ITO clay mixed with oxygen adsorbats (see EDS results), which can induce electric dipoles that could also contribute to enhancement of THz emission through strengthening the local field [43]. Apart from photo carriers under optical excitation, the built-in-potential in ITO/SI-GaAs interface may enhance further to contribute additional THz radiation due to electric dipoles generated by those extra adsorptions. The thickness of ITO thin film was also measured with cross-sectional SEM imaging. This is shown in Figure 2b. The prominent cleavage plane indicated a uniform ~243 nm-thick ITO film that was grown on the SI-GaAs substrate.

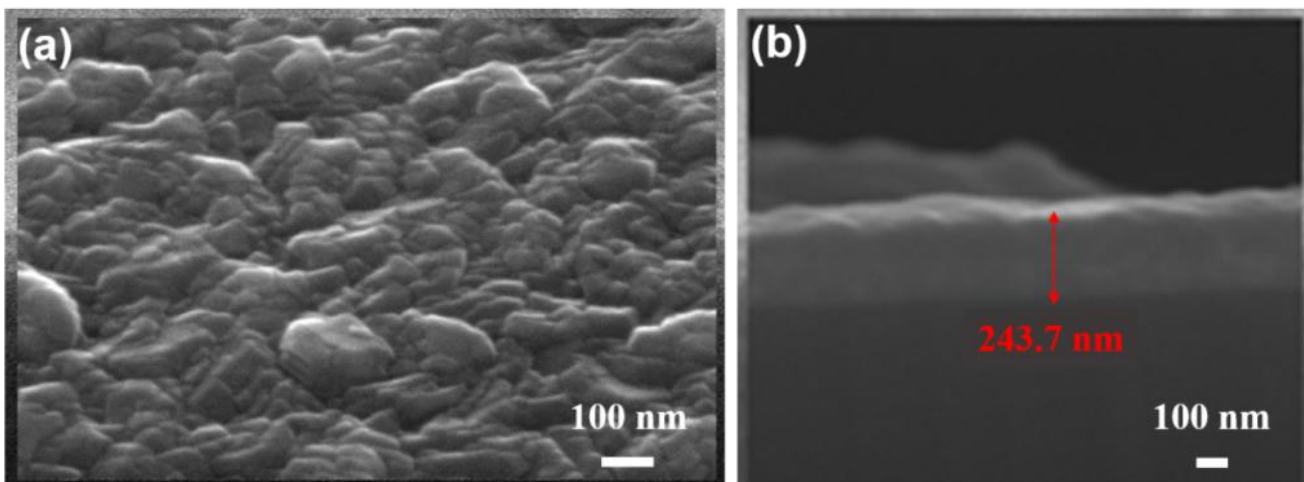


Figure 2. SEM images of ITO thin film with (a) top and (b) cross-sectional view.

Further, the elemental compositions of the ITO thin film were examined using energy-dispersive spectroscopy (EDS). This is displayed in Figure 3a. The acquired spectra revealed the existence of indium (In), tin (Sn), and oxygen (O) in the e-gun deposited ITO thin film. The weight percentage of In, Sn, and O is 68.91%, 7.27%, and 23.82%, respectively, whereas, the atomic percentage of In, Sn, and O is 27.91%, 2.85%, and 69.24%, respectively. The surface topography of the ITO thin film was also characterized using AFM as shown in Figure 3b. The average and root mean square (RMS) roughnesses of the thin film are 25.1 and 30.5 nm, respectively. Such high degree of roughness of the ITO thin film can provide a wide range of opportunities for roughness-induced, plasmon-assisted absorption of exciting optical radiation at the metal/semiconductor interface [44,45]. In related work, Wu et al. [38] showed that enhanced THz emission can be observed from GaAs (100) surfaces coated with thin (3–20 nm), inhomogeneous, and rough Au film.

The frequency-dependent THz optical constants of SI-GaAs and ITO thin film are shown in Figure 4. The theoretical formulism to estimate real (n) and imaginary (κ) refractive indices for both bulk semiconductor and nanoscale thin film have been reported earlier by our group [26,46]. Figure 4a shows that n is 3.65 for the SI-GaAs substrate and is relatively non-dispersed in the frequency range of 0.2 to 1.2 THz. On the other hand, we observed a negligible but non-zero (~ 0.005) extinction coefficient κ for the SI-GaAs substrate in the same frequency band. Such estimated values are consistent with those reported in previous works [46,47]. The n and κ of pristine ITO thin film (by itself, not combined with those of the substrate) varied from 97 to 47 and 80 to 27, respectively, in the frequency range of 0.2 to 1.2 THz (see Figure 4b). The monotonically decreasing trend of these optical constants with increasing frequencies in this band is mainly associated with frequency dependence of free carrier absorption in the material. The THz optical constants of the e-gun deposited ITO thin film determined in this work are also in agreement with

previously reported values of ITO thin films prepared by either DC reactive magnetron sputtering or pulsed laser deposition [46,47].

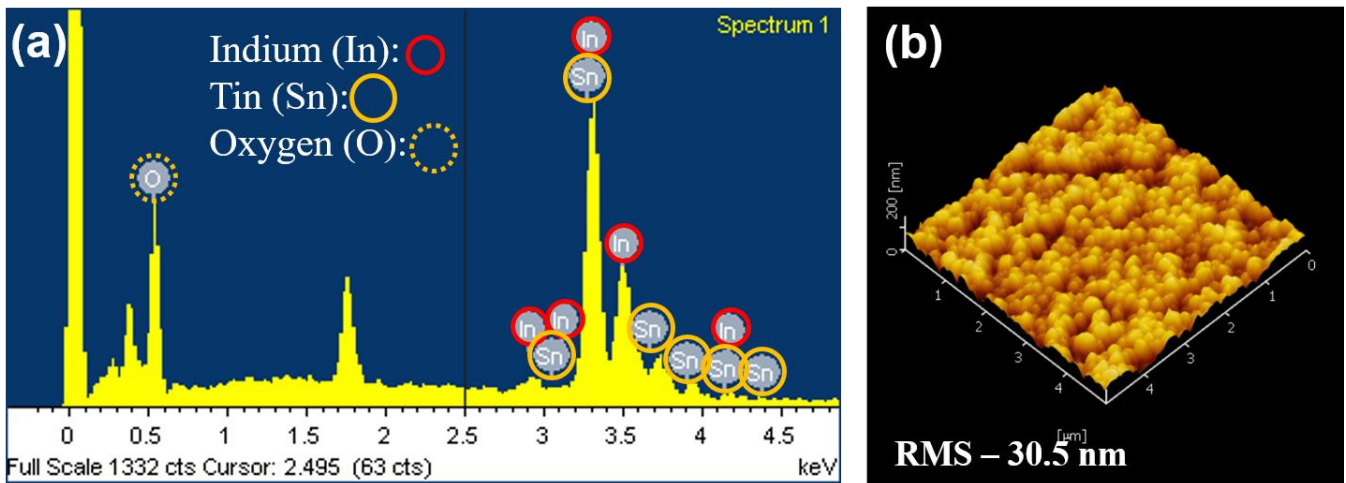


Figure 3. (a) EDS and (b) AFM images of ITO thin film.

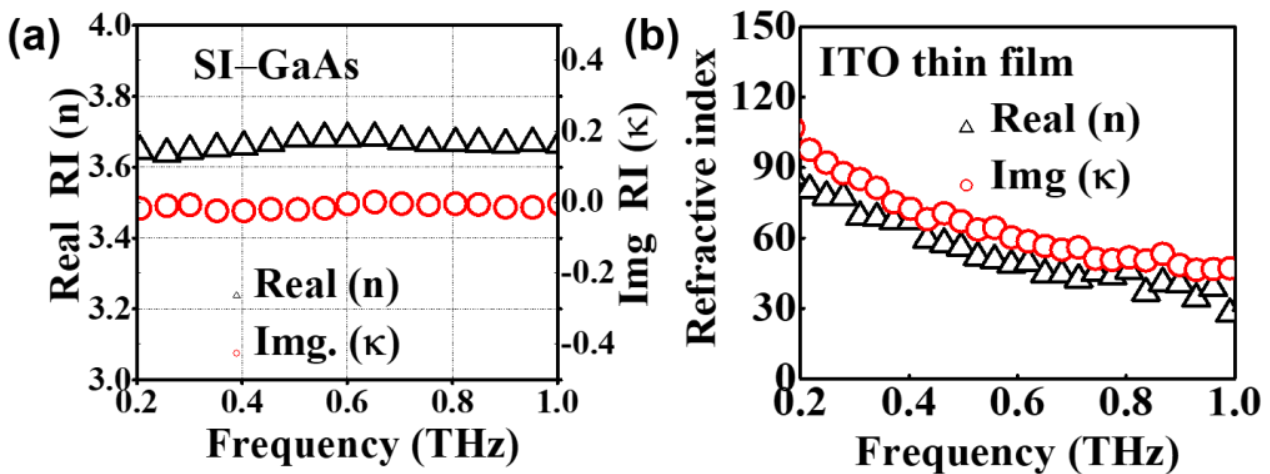


Figure 4. The real (n) and imaginary (κ) refractive indices as function of THz frequencies for (a) SI-GaAs and (b) ITO thin film.

The pump power dependence of THz emission from the SI-GaAs substrate and ITO/SI-GaAs sample are shown in Figure 5a. It is well-known that the physical mechanisms for optically excited THz emission from semiconductor and metal surfaces are predominantly either transient photocurrent or the optical rectification effect, at moderate optical pump intensities. The emitted THz field amplitude is $E_{\text{THz}} \propto \partial^2 P / \partial t^2$ or $\partial J / \partial t$, where P is the nonlinear polarization and J is the transient photocurrent density. The rate of change of J is proportional to built-in field at the ITO/GaAs Schottky interface (Appendix A.4), which arises from carrier depletion near the interface. The two mechanisms can be differentiated by examining the dependence of emitted field amplitude as a function of the pump intensity. The pump power dependence of THz emission from the SI-GaAs substrate and ITO/SI-GaAs sample are shown in Figure 5a. The incident angle of 35° and polarization angle of 0° of the excitation optical pulse were fixed.

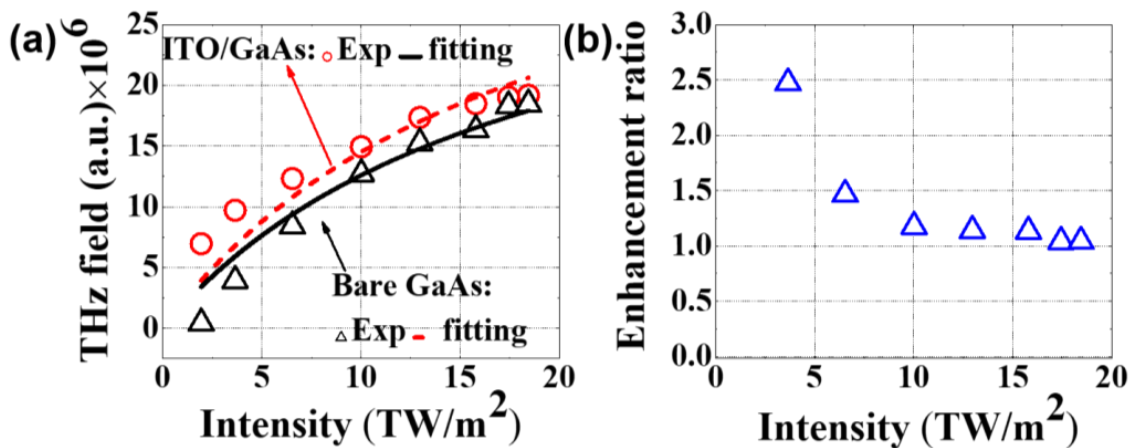


Figure 5. Optical pump intensity dependence. (a) THz emission from SI-GaAs and ITO/SI-GaAs and (b) emission enhancement ratio.

For a strictly second-order nonlinear optical effect (Appendix A.6), $E_{THz} \propto I_{pump}$. On the other hand, current surge tends to be saturated at high pump intensities. This is primarily attributed to the electrostatic screening by photocarriers generated at the surface region. In this model, the experimental results can be fitted theoretically using the following formula [48,49].

$$E_{THz} = A \frac{I_p}{I_p + I_s} \tag{1}$$

where A is the fixed scaling factor and I_s is the saturated optical pump power. The fitting curves are also shown in Figure 5a, which suggests that THz emission is mainly due to the surge current in the depletion zone near the ITO/GaAs interface. Discrepancies could be contributed by the optical rectification effect.

Figure 5b represents the THz enhancement ratio at different intensities of optical pump. The results indicate that the THz emission from the ITO/SI-GaAs sample is enhanced as high as 2.5 times at the minimum pump intensity of 3.6 TW/m² as that by the SI-GaAs substrate. This is much higher than those reported by previous works (1.5 times). The THz waveforms and corresponding spectra of THz radiation emitted by the bare SI-GaAs substrate and ITO/GaAs sample at low pump intensities are shown in Figure 6. The enhancement is prominent at the incident angle of 35°, polarization angle of 0°, and a very low but non-zero pump intensity.

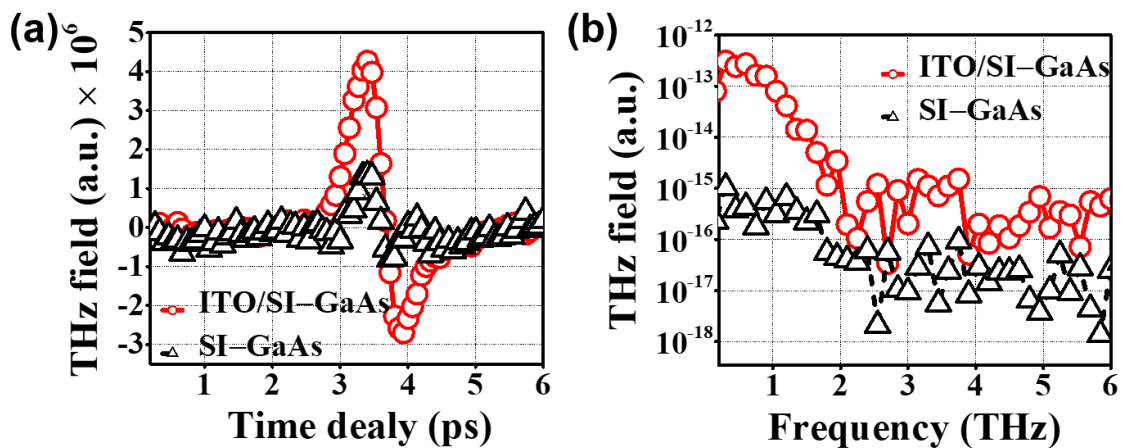


Figure 6. (a) THz waveforms and (b) corresponding spectra of THz radiation emitted by the bare SI-GaAs substrate and ITO/GaAs sample at low pump intensities.

THz waves can emit from air/GaAs or ITO/GaAs interfaces either in the forward or backward directions. The constructive interference between forward and retro-reflected backward THz waves will lead to enhancement of radiation in the forward direction [36]. However, calculations show that the effect is smaller than the observed enhancement.

Surface characterization by AFM showed that the ITO surface exhibits random, nanoscaled “islands”. Such features have been identified in numerous previous works either experimentally or in numerical simulations as material characteristics that can enhance the surface-plasmon-induced local field [38,44,50]. As a result, the field-induced surge current that is responsible for THz radiation would be enhanced. Additionally, the enhancement of THz emission with ITO thin film is reduced to zero (enhancement ratio of 1) when the intensity of pump power is over 17 TW/m². This can be explained with built-in-potential at the ITO/SI-GaAs interface. The number of photocarriers increases while strength of the built-in-potential at the interface decreased with increasing pump intensities [48,49]. As a result, thus the enhancement ratio trends to 1.

Figure 7a shows the emitted THz field amplitude for the exciting beam incident at angles from 0° to 50°. In this experiment, the optical pump intensity of 3.6 TW/m² and polarization angle of 0° was kept a constant. Note that no THz emission was observed from bare SI-GaAs substrate at near normal incidence, as expected for GaAs (100) surface. The peak amplitude of emitted THz radiation for both specimens under study increased monotonically as the incident angle was varied from 10° to 50°. The trend is in general agreement with a model first proposed by Auston and Zhang groups [49,51]. This is based on far-field dipole radiation by the surge current from a dipole layer at either the air/GaAs and ITO/GaAs interfaces, considering refraction at these interfaces according to Snell’s law. Similar angular dependence was recently reported for a layered tungsten disulfide crystal [52]. THz field in the forward direction can be expressed as:

$$E_{THz} = K \left[1 - \left(\frac{\tan(\theta_p - \theta_m)}{\tan(\theta_p + \theta_m)} \right)^2 \right] \sin(\theta_p) \times \frac{2 \cos(\theta_p) \sin(\theta_m)}{\sin(\theta_p + \theta_m) \cos(\theta_p - \theta_m)} \quad (2)$$

where K is a fitting constant; θ_p is the incident angle of optical pulses and $\theta_m = \sin^{-1}[\sin \theta_p / n_2]$; and n_2 is the THz refractive index of the medium. The theoretical curves using Equation (2) fit well with our experimental data. Our results on incidence-angle dependence are also consistent with previous works on Au/GaAs [37,38]. Note that Wu et al. [38] employed a very thin Au layer (3–20 nm) and found that THz emission saturated for Au film thicker than 8 nm. In comparison, our ITO film is much thicker (~240 nm). At normal incidence, however, the enhancement shown by our sample at normal incidence is several times larger than that of Wu et al. [38].

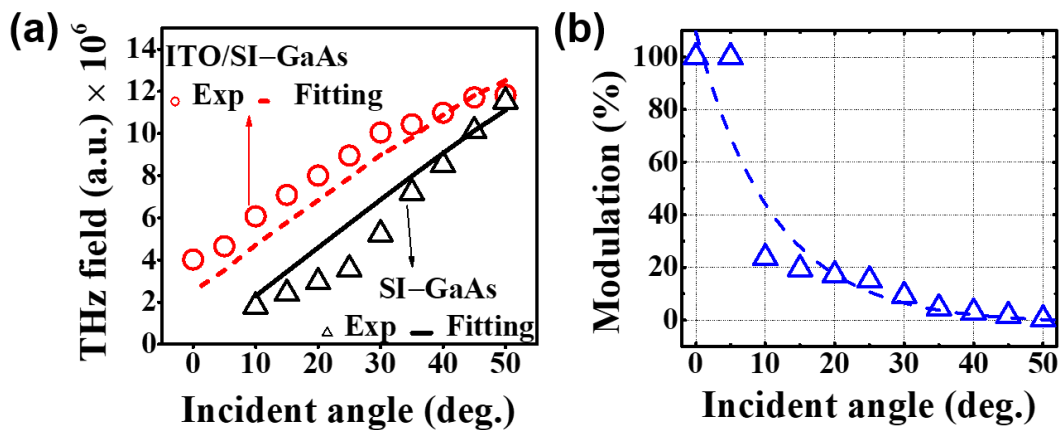


Figure 7. Optical pump incident angle dependence. (a) THz emission from SI-GaAs and ITO/SI-GaAs and (b) enhancement modulation with ITO/SI-GaAs sample.

To gain more insight, we further represented enhancement of emitted THz power by the ITO/SI-GaAs sample over that of the bare substrate in terms of modulation and expressed as

$$\text{Modulation} = \frac{E_{\text{THz(ITO/SI-GaAs)}} - E_{\text{THz(SI-GaAs)}}}{E_{\text{THz(ITO/SI-GaAs)}}} \times 100\% \quad (3)$$

which was plotted as a function of the incident angle in Figure 7b. The modulation was found to decrease exponentially with increasing incident angle. Note that a 100% modulation of THz emission was observed for the case of normal incidence. Additionally, the THz emission reached the maximum (data is not shown here) for both cases at the incident angle of 65° , which is close to the Brewster's angle of GaAs [52]. The null enhancement of THz emission at larger incidence angles of 50° further suggests that the angle-dependent photocurrent at the depletion layer is approximately the same for both cases [52].

Finally, we explored the dependence of THz emission on the polarization angle of laser pulses exciting both type of samples under study. This is shown in Figure 8. A HWP was inserted to tune the polarization angle of the incident laser pulse. The *p*-polarization and *s*-polarization are identified for polarization angles of 0° and 90° , respectively. The polarization angle was varied from 0° to 180° , while the pump intensity and incident angle were set at 3.6 TW/m^2 and 10° , respectively. It is well-known that the ZnTe-based electro-optic sampling (EOS) is sensitive to the polarization of the incident THz wave. In order to calculate precisely the amplitude of the THz field, this effect must be allowed for, e.g., by following the analysis of Chen et al. [53]. In our study of the effect of polarization dependence on THz emission, the aim was to determine whether a nonlinear optical effect, i.e., optical rectification, contributes to the THz signal. Since the sinusoidal dependence on polarization angle is already evident from the data (see Figure 8), we have not gone through the analysis.

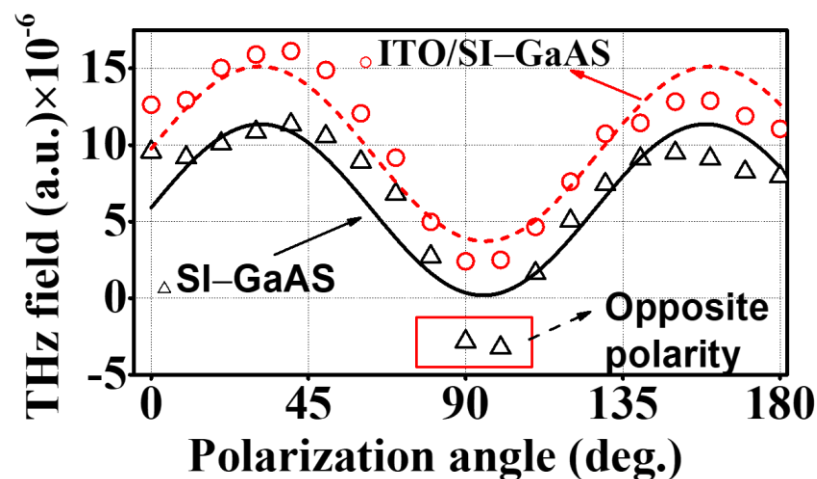


Figure 8. THz electric field dependence on polarization angle at fixed pump intensity and incidence angle.

The experimental data followed the expected sinusoidal dependence. However, the locations of the peaks and valleys as well as the period do not agree with the prediction using the theory of optical rectification (not shown). Similar characteristics of polarization angle dependence were reported by Huang et al., who studied a layered two-dimension (2D) material [21]. Additionally, Figure 8 shows that the THz emission waveform by the bare SI-GaAs reverses its polarity when the polarization angle is near 90° . This is consistent with previous works [12–17]. Further experiments show that this phenomenon occurs at $\sim 88^\circ$, the polarization angle for the air–GaAs interface. On the other hand, polarity reversal was not observed for the ITO/SI-GaAs.

Interestingly, the THz time domain signal exhibits two peaks at such angle. This is shown in Figure 9 for polarization angles of 80° and 90° . The corresponding THz power spectra also exhibit two peaks (not shown here). At this time, we cannot explain the phenomena.

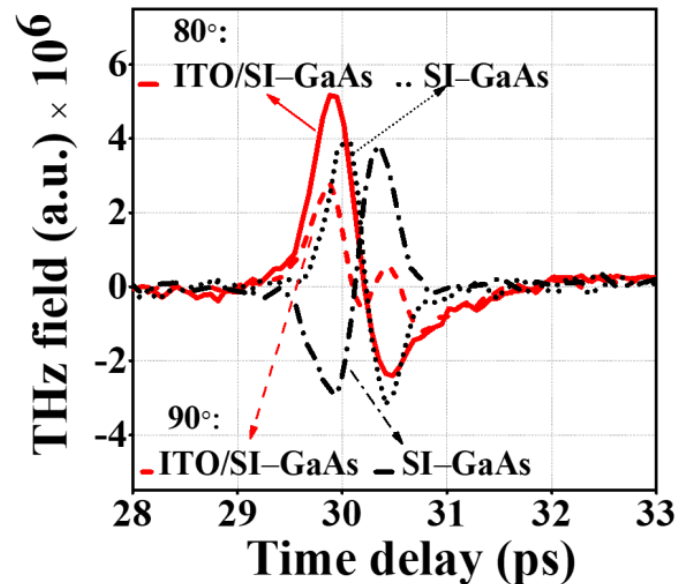


Figure 9. THz waveforms emitted by the bare GaAs substrate and ITO/GaAs sample at polarization angles of 80° (solid line for ITO/SI-GaAs and short dots for SI-GaAs) and 90° (short dash for ITO/SI-GaAs and short dash dots for SI-GaAs).

Previous works have attributed the polarity reversal for GaAs and Au/GaAs as the reversal of the interface transient current for such samples pumped at high power [35,36]. That is, the photoelectrons transported into GaAs from metal can tunnel back from GaAs into metal. The transient current induced by movement of such carriers is opposite to that of the photo-excited carrier generated in the surface depletion field of bare SI-GaAs [37]. The Schottky barrier height of ITO/GaAs and Au/GaAs is 0.678 eV and 0.33 eV, respectively [54,55]. Thus, it is much more difficult for electrons to tunnel through the ITO/GaAs interface. Further, ITO is a wide-bandgap material ($E_g \sim 3.5$ eV). It requires absorption of three or more NIR photons (~ 800 nm or 1.55 eV) to generate electrons and holes. Most of the incident photons would be injected into GaAs. There are also much less free carriers in ITO (resistivity, $\rho \sim 10^{-4} \Omega\cdot\text{cm}$) than metals ($\rho \sim 2.44 \times 10^{-8} \Omega\cdot\text{m}$). As a result, the free electron absorption phenomenon in ITO is significantly smaller than that in Au. Thus, our negative observation of polarity flip for ITO/GaAs versus GaAs is reasonable.

Following the above arguments, we propose that the THz signals measured from the ITO/GaAs sample should be emitted by the ITO/GaAs interface. Through our studies of the dependence of emitted THz field on incident angle, pump power, and polarization angle, we can conclude that both interface-field-induced transient current and field-induced optical rectification contribute to the observed signal. Taking into account surface characteristics of our samples revealed by SEM and AFM, we propose that surface-plasmon-induced local field is mainly responsible for the observed enhancement. This is corroborated by numerous previous works either experimentally or in numerical simulations on the enhancement effect [29,33,38,50,56]. Oxygen adsorbents in the ITO thin film also contributes to the enhancement. The process is also aided by constructive interference of forward and retro-reflected backward THz waves.

On the other hand, many physical mechanisms, such as optical rectification, diffusion current (photo-Dember effect), or drift current due to the built-in electric field, can contribute to the polarization angle dependence of THz emission from semiconductors such as ITO and GaAs [57,58]. The photo-Dember effect can be ruled out for the samples under study, for these possess wide bandgaps. The built-in electric field induced in the depletion region of the semiconductor can lead to band bending that generates the opposite movement of electron-hole, and thereby modified the polarization angle dependence of THz emission.

It is well-known that the surface morphology of ITO thin films would affect its optical and structural properties and performance in devices. Post-deposition annealing, either in a tube furnace [59,60] or rapid thermal annealing (RTA) [61,62], is an effective and widely used method to improve electrical and optical properties of ITO films. The root mean square roughness (rms) of the ITO film after either furnace annealing or RTA were found to be larger than that of the as-deposited film. This is commonly attributed to the larger crystallite size of ITO after annealing. Pretreatment, either chemical or by oxygen plasma treatment, will also make the surface rougher [63]. However, the treated surfaces are comparatively smoother than those annealed. Based on our results and those in previous works, we expect that the ITO thin film post-annealed under optimum conditions may lead to further enhancement of THz radiation from ITO-coated semiconductor surfaces. It is also expected that nanostructured ITO would also enhance THz emission for the semiconductor being coated. In future work, we will study the system with various thicknesses of ITO coating as well as nanostructured ITO, with pre-treatment or post annealing. This could help in elucidating the true nature of the enhancement.

4. Conclusions

In this study, we report enhancement of terahertz (THz) radiation with relatively thick indium-tin-oxide (ITO) thin-film deposited by e-gun evaporation on semi-insulating gallium arsenide substrate (SI-GaAs). The field amplitudes of THz emission from both ITO/SI-GaAs and bare SI-GaAs substrate as a function of (i) incident angle, (ii) polarization angle, and (iii) power of optical pump were investigated. Using a transmission type emission setup, the enhancement of peak amplitude of THz pulses transmitted through the ITO/SI-GaAs sample in comparison to bare SI-GaAs substrate were varied from 100% to 0% when the pump incidence angle changed from 0° to 50°. The maximum enhancement ratio of peak amplitude for coated sample to the bare substrate was approximately 2.5 times at the minimum pump intensity of 3.6 TW/m² and gradually decreased to one at the maximum pump intensity employed of 20 TW/m². From outcomes of these studies, together with surface and material characterization of the samples by SEM, AFM, EDS and THz-TDS, we show that THz emission originates from the ITO/GaAs interfaces. Further, both interface-field-induced transient current and field-induced optical rectification contribute to the observed THz signal. Observed enhancement was tentatively attributed to surface-plasmon-induced local field enhancement, coupled with constructive interference of forward and retro-reflected backward THz emission from the ITO/GaAs interfaces. The polarity-flip reported previously for very thin Au-coated GaAs was not observed. This was explained by the wide-bandgap, transparency and lower free carriers of ITO. For best results, the incident angle should be in the range of 0 to 30° and the incident polarization should be 0 to 45°. We further predict that the ITO thin film of suitable thickness or with engineered nanostructures, post-annealed under optimum conditions may lead to further enhancement of THz radiation from ITO-coated semiconductor surfaces.

Author Contributions: Conceptualization, C.-L.P.; methodology, A.K.S., S.-Y.K., and C.-L.P.; software, S.-Y.K.; validation, A.K.S., S.-Y.K., and C.-L.P.; formal analysis, A.K.S., S.-Y.K., and C.-L.P.; investigation, A.K.S., S.-Y.K., and C.-L.P.; resources, P.Y. and C.-L.P.; data curation, A.K.S. and S.-Y.K.; writing—original draft preparation, A.K.S.; writing—review and editing, C.-L.P.; supervision, C.-L.P.; funding acquisition, C.-L.P. All authors have read and agreed to the published version of the manuscript.

Funding: This research was funded by the Ministry of Science and Technology, Taiwan, under various grants.

Institutional Review Board Statement: Not applicable.

Informed Consent Statement: Not applicable.

Data Availability Statement: The data presented in this study are available on request from the corresponding author.

Acknowledgments: A.K.S. would like to thank Wei-Cheng Au for fitting Figure 7a.

Conflicts of Interest: The authors declare no conflict of interest.

Appendix A

Appendix A.1 Built-In Field

A built-in field or built-in-potential can exist at the interface or junction of any two different materials. This could result from unequal dopant concentration in the two materials. A built-in field can also be due to band bending at surfaces or interfaces that leads to the formation of a depletion region of carriers. This the case for the system under study in this work.

Appendix A.2 Dipole Radiation

The electromagnetic flux emitted by the electric dipole of oscillation is referred to as dipole radiation. In the far-field dipole radiation model for the surface THz emission, the radiated THz field can be written as:

$$E_{\theta} = \left(\frac{\sin \theta}{4\pi\kappa c^2} \right) \int_s \frac{\dot{J}_s}{|r - r'|} ds'$$

where θ is the angle between the emitted THz wave propagation and particle (carrier) acceleration direction; \dot{J}_s is the retarded photocurrent density generated by charge carrier with optical pulse while incident on the semiconductor surface; κ is the dielectric constant of the illuminated surface; c is the speed of light in vacuum; and s' is the excitation area.

Appendix A.3 Lateral Photo-Dember Current

This is an effective means of generating THz radiation by taking advantage of the effective photovoltage developed by the with a strong spatial gradient. When a highly absorbing (narrow-bandgap) semiconductor surface is optically excited, a carrier gradient would be developed perpendicular to the surface, because of the much faster diffusion of electrons than holes that are generated. After a short time depending on the carrier gradient and the carrier densities, this space-charge field couples the diffusion of electrons and holes giving rise to a transient ambipolar diffusion current that radiates electromagnetic transient in the THz frequency range. This phenomenon is named the Photo-Dember effect. A strong carrier gradient can also be achieved at the edge of a metalized stripe, resulting in a photo-Dember effect parallel to the surface, i.e., a lateral Photo-Dember Current.

Appendix A.4 Metal/Semiconductor Schottky Interface

A potential energy barrier for electrons formed at the junction between metal and semiconductor. This is dependent on the work function of the metal and described as:

$$\phi_{bi} = q\phi_{bn} - KT \ln \frac{N_c}{N_d}$$

where ϕ_{bn} is the metal work function and N_c is the electron density in the conduction band of the semiconductor.

Appendix A.5 Optical Rectification

This phenomenon arises from frequency mixing of the modes in ultrafast optical pulses with a spectrum spanning tens of THz that leads to frequency mixing in the “dc” range. As a result, ultrafast electromagnetic transients whose spectrum lies in the THz frequency band are generated. The nonlinear optical response could be caused by second-order susceptibility in non-centrosymmetric crystals and/or third-order one induced by an effective second-order susceptibility that is assisted by the built-in field (Appendix A.1) present at semiconductor surfaces or semiconductor/metal interfaces. The THz field due to optical rectification can be expressed as:

$$E_{\text{THz}} \approx \frac{4\pi WS}{Rc^3 n \alpha \tau_i^3} \left(\chi^{(2)} + \alpha \chi^{(3)} \int_0^{\infty} F e^{-\alpha z} dz \right)$$

where $\chi^{(2)}$ and $\chi^{(3)}$ are second- and 3rd-order nonlinear optical susceptibilities, W is the fluence of the exciting radiation; S is the area of the laser excited spot on the semiconductor surface; R is the distance from the point of observation to the emitting region; n is the refractive index of medium at the wavelength of the exciting radiation; α is the optical absorption coefficient; F is the electric field induced by the spatial separation of photocarriers; c is the speed of light in vacuum; τ_i is the laser pulse duration

Appendix A.6 Second-Order Nonlinear Optical Effect

This is the lowest order of nonlinear optical process in non-centrosymmetric material systems. Due to this effect, two input waves can mix to produce a third wave. Well-known 2nd-order nonlinear optical effects include second harmonic generation, sum frequency generation and difference frequency generation, or optical rectification (see Appendix A.5).

Appendix A.7 Surge Current

A surge or transient current arises when photogenerated carriers are accelerated in a field provided by, e.g., a biased photoconductive antenna. In lieu of the bias, a built-in field at the surface or interfaces could also accelerate the carriers. The resultant current surge, ultrashort in time scale, is the source term in Maxwell's equations that governs the radiation of electromagnetic transient, i.e., THz pulse.

Appendix A.8 Surface Plasmons

Surface plasmons (SPs) are collective or coherent delocalized electron oscillations that exist at the interface between any two materials where the real part of the dielectric function changes sign across the interface, e.g., a metal-dielectric interface, such as that between ITO and GaAs in this study. For the relatively rough ITO surface, surface plasmons are confined to wavelength-scaled features of the film, greatly enhancing the local field near the nanoscaled structure.

Appendix A.9 Transient Photocurrent

The transient photocurrent is the alternative name for surge current (See Appendix A.7). Besides the mechanisms discussed in Appendix A.7, 2D materials under obliquely incident illumination can generate electrons and holes that are distributed asymmetrically along the center of the Dirac cone. This drives photo-induced carrier motions and produces transient net current through the junction, which result in THz wave radiation.

References

1. Lee, Y.-S. *Principles of Terahertz Science and Technology*, 1st ed.; Springer: New York, NY, USA, 2009.
2. Koul, S.K.; Kaurav, P. *Sub-Terahertz Sensing Technology for Biomedical Applications*; Springer: Singapore, 2022.
3. Woolard, D.L.; Jensen, J.O.; Hwu, R.J.; Shur, M.S. *Terahertz Science and Technology for Military and Security Applications*; World Scientific: Hackensack, NJ, USA, 2007.

4. Pavlidis, D. *Fundamentals of Terahertz Devices and Applications*; John Wiley & Sons: Hoboken, NJ, USA, 2021.
5. Editors: Ghzaoui, M.E.; Das, S.; Lenka, T.R.; Biswas, A. *Terahertz Wireless Communication Components and System Technologies*; Springer International Publishing AG: Cham, Switzerland, 2022.
6. Nagatsuma, T.; Hisatake, S.; Fujita, M.; Pham, H.H.N.; Tsuruda, K.; Kuwano, S.; Terada, J. Millimeter-wave and terahertz-wave applications enabled by photonics. *IEEE J. Quantum Electron.* **2015**, *52*, 0600912. [[CrossRef](#)]
7. Fager, C.; Member, S.; Eriksson, T.; Member, S.; Fellow, H.Z.; Dielacher, F.; Member, S.; Studer, C.; Member, S. Implementation Challenges and Opportunities in Beyond-5G and 6G Communication. *IEEE J. Microw.* **2021**, *1*, 1–14.
8. Ahmad, Z.; Choi, W.; Sharma, N.; Zhang, J.; Zhong, Q.; Kim, D.-Y.; Chen, Z.; Zhang, Y.; Han, R.; Shim, D.; et al. Devices and circuits in CMOS for THz applications. In Proceedings of the 2016 IEEE International Electron Devices Meeting (IEDM), San Francisco, CA, USA, 3–7 December 2016.
9. Akyildiz, I.F.; Han, C.; Hu, Z.; Nie, S.; Jornet, J.M. Terahertz band communication: An old problem revisited and research directions for the next decade. *IEEE Trans. Commun.* **2022**, *70*, 4250–4285. [[CrossRef](#)]
10. Krishna, M.G.; Kshirsagar, S.D.; Tewari, S.P. Terahertz emitters, photodetector, Chapter 6. In *Detectors and Sensors: Current Status and Future Prospects*; Gateva, S., Ed.; IntechOpen: London, UK, 2012; pp. 115–144.
11. Carpinero, G. *Semiconductor Terahertz Technology: Devices and Systems at Room Temperature Operation*; Wiley-IEEE Press: New York, NY, USA, 2015.
12. Köhler, R.; Tredicucci, A.; Beltram, F.; Beere, H.E.; Linfield, E.H.; Davies, A.G.; Ritchie, D.A.; Iotti, R.C.; Rossi, F. Terahertz Semiconductor-Heterostructure Laser. *Nature* **2002**, *417*, 156–159. [[CrossRef](#)] [[PubMed](#)]
13. Faist, J.; Capasso, F.; Sivco, D.L.; Sirtori, C.; Hutchinson, A.L.; Cho, A.Y. Quantum Cascade Laser. *Science* **1994**, *264*, 553–556. [[CrossRef](#)] [[PubMed](#)]
14. Ramakrishnan, G.; Kumar, N.; Ramanandan, G.K.P.; Adam, J.L.A.; Hendrikx, W.A.R.; Planken, C.M.P. Plasmon-Enhanced Terahertz Emission from a Semiconductor/metal Interface. *Appl. Phys. Lett.* **2014**, *104*, 071104. [[CrossRef](#)]
15. Huang, Y.; Zhu, L.; Yao, Z.; Zhang, L.; He, C.; Zhao, Q.; Bai, J.; Xu, X. Terahertz Surface Emission from Layered MoS₂ Crystal: Competition between Surface Optical Rectification and Surface Photocurrent Surge. *J. Phys. Chem. C* **2018**, *122*, 481–488. [[CrossRef](#)]
16. Huang, Y.; Yao, Z.; He, C.; Zhu, L.; Zhang, L.; Bai, J.; Xu, X. Terahertz Surface and Interface Emission Spectroscopy for Advanced Materials. *J. Phys. Condens. Matter* **2019**, *31*, 153001. [[CrossRef](#)]
17. Dekorsy, T.; Pfeifer, T.; Kütt, W.; Kurz, H. Subpicosecond carrier transport in GaAs surface-space-charge fields. *Phys. Rev. B Condens. Matter Mater. Phys.* **1993**, *47*, 3842. [[CrossRef](#)]
18. Krotkus, K.; Adomavicius, R.; Malevich, V.L. Terahertz emission from semiconductors excited by ultrafast laser pulses. In *Terahertz Frequency Detection and Identification of Materials and Objects*; Miles, R.E., Zhang, X.-C., Eisele, H., Krotkus, A., Eds.; Springer: Berlin/Heidelberg, Germany, 2007.
19. Gu, P.; Tani, M. Terahertz radiation from semiconductor surfaces. In *Terahertz Optoelectronics*; Sakai, K., Ed.; Springer: Berlin/Heidelberg, Germany, 2005.
20. Ramanandan, G.K.P.; Ramakrishnan, G.; Kumar, N.; Planken, P.; Adam, A.J.L. Emission of terahertz pulses from nanostructured metal surfaces. *J. Phys. D Appl. Phys.* **2014**, *47*, 374003. [[CrossRef](#)]
21. Huang, Y.; Zhu, L.; Zhao, Q.; Guo, Y.; Ren, Z.; Bai, J.; Xu, X. Surface Optical Rectification from Layered MoS₂ Crystal by THz Time-Domain Surface Emission Spectroscopy. *ACS Appl. Mater. Interfaces* **2017**, *9*, 4956–4965. [[CrossRef](#)]
22. Fan, Z.; Xu, M.; Huang, Y.; Lei, Z.; Zheng, L.; Zhang, Z.; Zhao, W.; Zhou, Y.; Wang, X.; Xu, X.; et al. Terahertz Surface Emission from MoSe₂ at the Monolayer Limit. *ACS Appl. Mater. Interfaces* **2020**, *12*, 48161–48169. [[CrossRef](#)] [[PubMed](#)]
23. Si, K.; Huang, Y.; Zhao, Q.; Zhu, L.; Zhang, L.; Yao, Z.; Xu, X. Terahertz Surface Emission from Layered Semiconductor WSe₂. *Appl. Surf. Sci.* **2018**, *448*, 416–423. [[CrossRef](#)]
24. Chopra, K.L.; Major, S.; Pandya, D.K. Transparent Conductors—A Status Review. *Thin Solid Film.* **1983**, *102*, 1–46. [[CrossRef](#)]
25. Ellmer, K. Past Achievements and Future Challenges in the Development of Optically Transparent Electrodes. *Nat. Photonics* **2012**, *6*, 809–817. [[CrossRef](#)]
26. Yang, C.S.; Chang, C.M.; Chen, P.H.; Yu, P.; Pan, C.L. Broadband terahertz conductivity and optical transmission of indium-tin-oxide (ITO) nanomaterials. *Opt. Express* **2013**, *21*, 16670–16682. [[CrossRef](#)] [[PubMed](#)]
27. Chen, C.-W.; Lin, Y.-C.; Chang, C.-H.; Yu, P.; Shieh, J.-M.; Pan, C.-L. Frequency-dependent complex conductivities and dielectric responses of indium tin oxide thin films from the visible to the far-infrared. *IEEE J. Quantum Electron.* **2010**, *46*, 1746–1754. [[CrossRef](#)]
28. Brown, E.R.; Zhang, W.D.; Chen, H.; Mearini, G.T. THz Behavior of Indium-Tin-Oxide Films on p-Si Substrates. *Appl. Phys. Lett.* **2015**, *107*, 091102. [[CrossRef](#)]
29. Ghobadi, H.; Smirnov, Y.; Offerhaus, H.L.; Alvarez-Chavez, J.A.; Morales-Masis, M.; De Leon, I. Optical properties of highly-crystalline tin-doped indium oxide films in their near-zero permittivity spectral region. *Opt. Mater. Express* **2022**, *12*, 96–108. [[CrossRef](#)]
30. Franzen, S.; Rhodes, C.; Cerruti, M.; Gerber, R.W.; Losego, M.; Maria, J.-P.; Aspnes, D.E. Plasmonic Phenomena in Indium Tin Oxide and ITO-Au Hybrid Films. *Opt. Lett.* **2009**, *34*, 2867–2869. [[CrossRef](#)]
31. Aithal, R.K.; Doss, A.T.; Kumaraswamy, D.P.; Mills, D.K.; Kuila, D. Growth and Functionality of Cells Cultured on Conducting and Semi-Conducting Surfaces Modified with Self-Assembled Monolayers (SAMs). *Coatings* **2016**, *6*, 9. [[CrossRef](#)]

32. Subacius, A.; Baloukas, B.; Bousser, E.; Hinder, S.J.; Baker, M.A.; Rebholz, C.; Matthews, A. Nanostructural Characterisation and Optical Properties of Sputter-Deposited Thick Indium TinOxide (ITO) Coatings. *Coatings* **2020**, *10*, 1127. [[CrossRef](#)]
33. Alam, M.Z.; De Leon, I.; Boyd, R.W. Large optical nonlinearity of indium tin oxide in its epsilon-near-zero region. *Science* **2016**, *352*, 795. [[CrossRef](#)] [[PubMed](#)]
34. Bhaskar, S.; Visweswar Kambhampati, N.S.; Ganesh, K.M.; Mahesh Sharma, P.; Srinivasan, V.; Ramamurthy, S.S. Metal-Free, Graphene Oxide-Based Tunable Soliton and Plasmon Engineering for Biosensing Applications. *ACS Appl. Mater. Interfaces* **2021**, *13*, 17046–17061. [[CrossRef](#)] [[PubMed](#)]
35. Jin, Y.; Ma, X.F.; Wagoner, G.A.; Alexander, M.; Zhang, X.C. Anomalous optically generated THz beams from metal/GaAs interfaces. *Appl. Phys. Lett.* **1994**, *65*, 682–684. [[CrossRef](#)]
36. Li, M.; Sun, F.G.; Wagoner, G.A.; Alexander, M.; Zhang, X.-C. Measurement and Analysis of Terahertz Radiation from Bulk Semiconductors. *Appl. Phys. Lett.* **1995**, *67*, 25–27. [[CrossRef](#)]
37. Shi, Y.; Yang, Y.; Xu, X.; Ma, S.; Yan, W.; Wang, L. Ultrafast Carrier Dynamics in Au/GaAs Interfaces Studied by Terahertz Emission Spectroscopy. *Appl. Phys. Lett.* **2006**, *88*, 161109. [[CrossRef](#)]
38. Wu, X.; Quan, B.; Xu, X.; Hu, F.; Lu, X.; Gu, C.; Wang, L. Effect of inhomogeneity and plasmons on terahertz radiation from GaAs (100) surface coated with rough Au film. *Appl. Surf. Sci.* **2013**, *285*, 853–857. [[CrossRef](#)]
39. Heyman, J.N.; Coates, N.; Reinhardt, A.; Strasser, G. Diffusion and Drift in Terahertz Emission at GaAs Surfaces. *Appl. Phys. Lett.* **2003**, *83*, 5476–5478. [[CrossRef](#)]
40. Sahoo, A.K.; Mai, C.-M.; Kang, S.-Y.; Yu, P.; Pan, C.-L. Studies of terahertz radiation from optically excited indium tin oxide / semi insulating gallium arsenide interface. In Proceedings of the 2020 45th International Conference on Infrared, Millimeter, and Terahertz Waves (IRMMW-THz), Buffalo, NY, USA, 8–13 November 2020.
41. Tsai, T.R.; Chen, C.Y.; Pan, C.L.; Pan, R.P.; Zhang, X.C. Terahertz time-domain spectroscopy studies of the optical constants of the nematic liquid crystal 5CB. *Appl. Opt.* **2003**, *42*, 2372–2376. [[CrossRef](#)]
42. Liu, T.A.; Tani, M.; Pan, C.-L. THz radiation emission properties of multi energy arsenic-ion-implanted GaAs and semi-insulating GaAs based photoconductive antennas. *J. Appl. Phys.* **2003**, *93*, 2996–3001. [[CrossRef](#)]
43. Bagsican, F.R.; Zhang, X.; Ma, L.; Wang, M.; Murakami, H.; Vajtai, R.; Ajayan, P.M.; Kono, J.; Tonouchi, M.; Kawayama, I. Effect of Oxygen Adsorbates on Terahertz Emission Properties of Various Semiconductor Surfaces Covered with Graphene. *J. Infrared Millim. Terahertz Waves* **2016**, *37*, 1117–1123. [[CrossRef](#)]
44. Goswami, S.; Sharma, A.K.; Biswas, S.; Alagarsamy, P. Evolution of epsilon-near-zero plasmon with surface roughness and demonstration of perfect absorption in randomly rough indium tin oxide thin films. *J. Appl. Phys.* **2021**, *130*, 173102. [[CrossRef](#)]
45. Ma, K.; Zhou, N.; Yuan, M.; Li, D.; Yang, D. Tunable surface plasmon resonance frequencies of monodisperse indium tin oxide nanoparticles by controlling composition, size, and morphology. *Nanoscale Res. Lett.* **2014**, *9*, 1–7. [[CrossRef](#)]
46. Yang, C.-S.; Lin, M.-H.; Chang, C.-H.; Yu, P.; Shieh, J.-M.; Shen, C.-H.; Wada, O.; Pan, C.-L. Non-Drude behavior in indium-tin-oxide nanowhiskers and thin films investigated by transmission and reflection THz time-domain spectroscopy. *IEEE J. Quantum Electron.* **2013**, *49*, 677–690. [[CrossRef](#)]
47. Wang, T.; Zalkovskij, M.; Iwaszczuk, K.; Lavrinenko, A.V.; Naik, G.V.; Kim, J.; Boltasseva, A.; Jepsen, P.U. Ultra broadband terahertz conductivity of highly doped ZnO and ITO. *Opt. Mat. Express* **2015**, *5*, 566. [[CrossRef](#)]
48. Reid, M.; Fedosejevs, R. Terahertz Emission from (100) InAs Surfaces at High Excitation Fluences. *Appl. Phys. Lett.* **2005**, *86*, 011906. [[CrossRef](#)]
49. Zhang, X.-C.; Hu, B.B.; Darrow, J.T.; Auston, D.H. Generation of femtosecond electromagnetic pulses from semiconductor surfaces. *Appl. Phys. Lett.* **1990**, *56*, 1011–1013. [[CrossRef](#)]
50. Huang, L.Y.; Zhang, L.; Zhou, J.Z.; Li, M.; Li, C.; Li, C.; Zhang, J.; Wang, S.; Zeng, H. Surface Plasmon Enhanced THz Emission with Nanoporous gold Supported CdTe. *Opt. Express* **2021**, *29*, 19853–19861. [[CrossRef](#)]
51. Zhang, X.C.; Auston, D.H. Optoelectronic Measurement of Semiconductor Surfaces and Interfaces with Femtosecond Optics. *J. Appl. Phys.* **1992**, *71*, 326–338. [[CrossRef](#)]
52. Zhang, L.; Huang, Y.; Zhao, Q.; Zhu, L.; Yao, Z.; Zhou, Y.; Du, W.; Xu, X. Terahertz Surface Emission of d-Band Electrons from a Layered Tungsten Disulfide Crystal by the Surface Field. *Phys. Rev. B Condens. Matter Mater. Phys.* **2017**, *96*, 155202. [[CrossRef](#)]
53. Chen, Q.; Tani, M.; Jiang, Z.; Zhang, X.-C. Electro-optic transceivers for terahertz-wave applications. *J. Opt. Soc. Am. B* **2001**, *18*, 823–831. [[CrossRef](#)]
54. Kim, H.S.; Park, M.S.; Kim, S.H.; Park, S.I.; Song, J.D.; Kim, S.H.; Choi, W.J.; Park, J.H. Indium-tin-oxide/GaAs Schottky barrier solar cells with embedded InAs quantum dots. *Thin Solid Film.* **2016**, *604*, 81–84. [[CrossRef](#)]
55. Halder, N.N.; Biswas, P.; Kundu, S.; Banerji, P. Au/p-Si Schottky junction solar cell: Effect of barrier height modification by InP quantum dots. *Sol. Energy Mater. Sol. Cells* **2014**, *132*, 230–236. [[CrossRef](#)]
56. Li, S.Q.; Guo, P.; Zhang, L.; Zhou, W.; Odom, T.W.; Seideman, T.; Ketterson, J.B.; Chang, R.P.H. Infrared Plasmonics with Indium–Tin–Oxide Nanorod Arrays. *ACS Nano* **2011**, *5*, 9161–9170. [[CrossRef](#)]
57. Mendis, R.; Smith, M.L.; Bignell, L.J.; Vickers, R.E.M.; Lewis, R.A. Strong Terahertz Emission from (100) p-Type InAs. *J. Appl. Phys.* **2005**, *98*, 126104. [[CrossRef](#)]
58. Tonouchi, M. Simplified formulas for the generation of terahertz waves from semiconductor surfaces excited with a femtosecond laser. *J. Appl. Phys.* **2020**, *127*, 245703. [[CrossRef](#)]

59. Morikawa, H.; Fujita, M. Crystallization and electrical property change on the annealing of amorphous indium-oxide and indium tin oxide films. *Thin Solid Films* **2000**, *359*, 61–67. [[CrossRef](#)]
60. Hanna, M.C.; Beard, M.C.; Nozik, A.J. Effect of Solar Concentration on the Thermodynamic Power Conversion Efficiency of Quantum-Dot Solar Cells Exhibiting Multiple Exciton Generation. *J. Phys. Chem. Lett.* **2012**, *3*, 2857–2862. [[CrossRef](#)]
61. Song, S.; Yang, T.; Liu, J.; Xin, Y.; Li, Y.; Han, S. Rapid thermal annealing of ITO films. *Appl. Surf. Sci.* **2011**, *257*, 7061–7064. [[CrossRef](#)]
62. Sahoo, A.K.; Mai, C.-M.; Pan, C.-L. Enhancement of Indium tin oxide nano-scale films for terahertz device applications treated by rapid thermal annealing. In Proceedings of the 2020 45th International Conference on Infrared, Millimeter, and Terahertz Waves (IRMMW-THz), Buffalo, NY, USA, 8–13 November 2020.
63. Khan, M.Z.H. Effect of ITO Surface Properties on SAM Modification: A Review Toward Biosensor Application. *Cogent Eng.* **2016**, *3*, 1170097. [[CrossRef](#)]

Disclaimer/Publisher’s Note: The statements, opinions and data contained in all publications are solely those of the individual author(s) and contributor(s) and not of MDPI and/or the editor(s). MDPI and/or the editor(s) disclaim responsibility for any injury to people or property resulting from any ideas, methods, instructions or products referred to in the content.